

## Computational Interpretation of Vibrational Optical Activity: The ROA Spectra of (4*S*)-4-Methylisochromane and the (4*S*)-Isomers of *Galaxolide*<sup>®</sup>

by Gérard Zuber and Werner Hug\*

Department of Chemistry, University of Fribourg, ch. du Musée 9, CH-1700 Fribourg

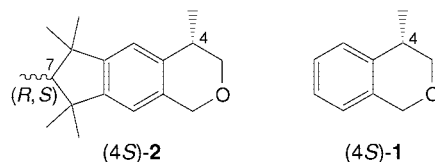
The reliable computation of *Raman*-optical-activity (ROA) spectra of molecules of the size of the title compounds has, until now, not been possible. We show that our rarefied basis sets yield results in good agreement with the experimental data for (4*S*)-4-methylisochromane (= (4*S*)-3,4-dihydro-4-methyl-1*H*-2-benzopyran; **1**), provided the equilibrium between the *pseudo*-equatorial and the *pseudo*-axial conformers is taken into account. Comparison between the measured and the computed ROA back-scattering spectra allows the unequivocal assignment of the absolute configuration of the molecule. Comparison with more-approximate calculations for the larger (4*S*)-isomers of *Galaxolide*<sup>®</sup> (**2**), which contain the (4*S*)-4-methylisochromane moiety, shows large-scale group frequencies on the same chiral fragments of the two molecules. The data confirm that ROA can be generated by interactions extending over several bonds, *i.e.*, over larger distances than can be probed by NMR spectroscopy. Thus, the absolute configuration at C(7) of *Galaxolide*<sup>®</sup> is assignable independently of that at C(4). The computation of ROA for forward-scattering, which will soon be measurable for *Galaxolide*<sup>®</sup>, suggests that this scattering geometry provides additional stereochemical information that will be valuable in situations where absolute configurations at several stereogenic centers have to be assigned.

**Introduction.** – *Raman* optical activity (ROA) [1–3] is a spectroscopic method with a very high sensitivity to the structural details of chiral molecules. This sensitivity is one of the major assets of the method, because molecules with closely related structures, which differ in minor details only, can readily be distinguished by their ROA spectra. Likewise, if a molecule exists in different conformations, then these conformations almost invariably lead to substantially differing ROA spectra. This extreme sensitivity to structural detail has, in the past, also been a headache, namely because the rules that permit the correlation of the size and the sign of observed ROA bands with the structure of a molecule are largely lacking. Though the information is clearly present in measured spectra, it has, therefore, only rarely been possible, without detailed computation, to deduce detailed structural information.

The advent of *ab initio* methods for computing molecular vibrations and molecular electronic tensors has led to a breakthrough in the understanding of ROA spectra [4–6]. The same holds true for ROA's sister method, vibrational circular dichroism (VCD) [7]. In the past, the computation of VCD has incurred less expense than that of ROA, and the interpretation of the VCD spectra of small molecules has, therefore, had a head-start over that of ROA. As a consequence, there exists a far larger body of experience on the computation of VCD than of ROA spectra, and some of the basic minimal requirements for the successful computation of ROA spectra have actually only recently been investigated [8].

For H-atom-containing organic molecules, it was found that small, rarefied basis sets [8] and the *Hartree–Fock* (*HF*) approach suffice for the determination of the electronic tensor part in ROA calculations of moderate precision. The reason is that it is mostly the gradients of electronic tensors on H-atoms that need to be well described, and that this can be accomplished with moderate computational expense. In contrast, for the vibrational part, the *HF* approach is inadequate, and electron correlation has to be taken explicitly into account. As for other molecular properties, where electron correlation cannot be neglected, density functional theory (DFT) has proved the most cost-effective approach [6]. These findings for vibrational modes are consistent with identical conclusions reached earlier in VCD [9]. For the electronic part, on the other hand, a similarly detailed investigation as for the electronic tensor part in ROA calculations has, so far, not been published for VCD.

The combination of calculations of the electronic tensor part by *HF* linear-response theory performed with rarefied basis sets, with a DFT calculation of vibrational modes done with more-comprehensive basis sets, provides, for the first time, the opportunity for computing ROA spectra of chiral molecules of actual chemical interest. In the present work, we exploit this for investigating the ROA properties of (4*S*)-4-methylisochromane (= (4*S*)-3,4-dihydro-4-methyl-1*H*-2-benzopyran; **1**)<sup>1</sup>). This molecule is of interest in itself, and it is also of interest because it represents the decisive chiral moiety of the (4*S*)-isomers of *Galaxolide*® (= 1,3,4,6,7,8-hexahydro-4,6,6,7,8,8-hexamethylindeno[5,6-*c*]pyran; **2**)<sup>2</sup>).



In view of the stereochemical interest [11] in *Galaxolide*®, and as it is, at present, not possible to compute molecules of such size with the same degree of precision achieved for **1**, we also present lower-quality computed spectra for these larger molecules. The conclusions drawn from these data of somewhat limited precision are validated by comparing results obtained at the same modest level of theory for **1** with the higher-quality results we have for this molecule, and by comparison with experimental data.

**Theory.** – The relevant molecular quantities for *Raman* and ROA scattering are the cross-sections and  $-\Delta\sigma$ , respectively, for scattering into a solid angle of  $4\pi$ . As we have shown, quadrupole contributions to ROA scattering vanish for an isotropic sample when scattering is summed over all directions [3]. In practical terms, it is difficult to actually sum scattering intensities over all scattering angles, and experimental results in *Raman* and ROA spectroscopy represent almost always

<sup>1</sup>) Prepared in 95% enantiomeric excess (ee) from commercially available (*S*)-2-phenylpropan-1-ol by means of a standard cyclization procedure [10].

<sup>2</sup>) The (4*S*,7*R*)- and (4*S*,7*S*)-diastereoisomers of **2** are the two olfactorily most-potent isomers of this compound and were provided by *Givaudan* in 96% ee. In the following, the 1:1 mixture of these diastereoisomers is simply referred to as ‘(4*S*)-*Galaxolide*’ or ‘(4*S*)-**2**’.

scattering intensities collected for a relatively small solid angle and for a specific scattering direction. The appropriate molecular quantities for this situation are the differential scattering cross sections  $d\sigma$  and  $-\Delta d\sigma$ .

*Raman* and ROA spectra measured for different scattering angles, or with different polarization schemes, do not, in general, provide identical information. The reason is that the linear combinations of the various scattering invariants, which appear below in *Eqns. 1* and *2*, for  $d\sigma$  and  $-\Delta d\sigma$  are different for different experimental arrangements. The identification [12], and, in particular, the elimination [13] of quadrupole contributions in ROA has in the past been of some interest when experimental data were compared with computed ones, because the computation of quadrupole contributions proved notoriously difficult. In view of the better understanding of the computational requirements for ROA [8], this has become less of a concern.

ROA Back- [14][15] and forward-scattering [16], which are favored in the present work, have the merit of representing pure anisotropic and almost pure isotropic scattering, respectively. We will demonstrate computationally the potential that forward-scattering might have for assigning absolute configurations from *ROA* spectra observed for low-frequency vibrational modes.

Within the *Placzek* polarizability theory, the differential *Raman* scattering cross-sections for forward- and back-scattering can be written in the scattered-circular-polarization (SCP) mode [17][18] as:

$$^n d\sigma(0)_{\text{SCP}} = ^n d\sigma(\pi)_{\text{SCP}} = K(90a^2 + 14\beta^2)d\Omega \quad (1)$$

For ROA, one has for forward-scattering

$$-\Delta^n d\sigma(0)_{\text{SCP}} = \frac{K}{c}(360aG' + 8\beta_G^2 - 8\beta_A^2)d\Omega \quad (2)$$

and for back-scattering

$$-\Delta^n d\sigma(\pi)_{\text{SCP}} = \frac{K}{c}(48\beta_G^2 + 16\beta_A^2)d\Omega \quad (3)$$

Here,  $\Omega$  is the solid angle, and  $K$  is a constant that depends on the frequency  $\omega_0$  of the exciting light, and on the frequency  $\omega_p$  of the scattered light, where  $p$  is the vibrational mode for which a transition between different vibrational states occurs (*Eqn. 4*).

$$K_p = \frac{1}{90} \left( \frac{\mu_0}{4\pi} \right)^2 \omega_p^3 \omega_0 \quad (4)$$

The invariants  $\alpha^2$ ,  $\beta^2$ ,  $aG'$ ,  $\beta_G^2$ , and  $\beta_A^2$  of the of *Raman* and ROA transition tensors [19] are:

$$a^2 = \frac{1}{9} \sum_{\mu,\nu} \alpha_{\mu\mu} \alpha_{\nu\nu} \quad (5a)$$

$$\beta^2 = \frac{1}{2} \sum_{\mu,\nu} (3\alpha_{\mu\nu} \alpha_{\mu\nu} - \alpha_{\mu\mu} \alpha_{\nu\nu}) \quad (5b)$$

$$aG' = \frac{1}{9} \sum_{\mu,\nu} \alpha_{\mu\mu} G'_{\nu\nu} \quad (5c)$$

$$\beta_G^2 = \frac{1}{2} \sum_{\mu,\nu} (3\alpha_{\mu\nu} G'_{\mu\nu} - \alpha_{\mu\mu} G'_{\nu\nu}) \quad (5d)$$

$$\beta_A^2 = \frac{\omega_0}{2} \sum_{\mu,\nu} \alpha_{\mu\nu} \mathcal{A}_{\mu\nu} \quad (5e)$$

Here  $a^2$  is the isotropic and  $\beta^2$  the anisotropic invariant of the electric-dipole/electric-dipole polarizability tensor, respectively;  $aG'$  and  $\beta_G^2$  are the isotropic and anisotropic invariants due to cross-products of this tensor with the electric-dipole/magnetic-dipole polarizability tensor, and  $\beta_A^2$  is the anisotropic invariant due to its cross-product with the tensor  $\mathcal{A}_{\mu\nu}$  obtained by contracting the electric-dipole/electric-quadrupole polarizability tensor with the antisymmetric-unit tensor of *Levi–Civita*. For a fundamental vibrational transition, *Eqns. 5a–e* can be written in the general form [3] [18]:

$$I_p = \frac{\hbar}{400\pi c \Delta \tilde{\nu}_p} \sum_{\alpha,\beta} \mathbf{L}_{\alpha,p}^x \cdot \mathbf{V}_{\alpha\beta} \cdot \mathbf{L}_{\beta,p}^x \quad (6)$$

where  $c$  is the speed of light and  $\Delta \tilde{\nu}_p$  the wavenumber shift (in  $\text{cm}^{-1}$ ) in the *Raman* spectrum.  $\mathbf{L}_{\alpha,p}^x$ , the *Cartesian* displacement vector of nucleus  $\alpha$  with mass  $m_\alpha$  in normal mode  $p$ , is normalized as follows:

$$\sum_{\alpha,i} m_\alpha (L_{\alpha i,p}^x)^2 = 1 \quad (7)$$

As an example of the form of the dyadics,  $\mathbf{V}_{\alpha\beta}$  [18], we give here their elements for the invariant  $aG'$ , which is responsible for isotropic ROA scattering, and for the

invariant  $\beta_G^2$ , which, in general, makes the largest contribution to anisotropic ROA scattering:

$$V(aG')_{ai\beta j} = \frac{1}{9} \sum_{\mu,\nu} \left( \frac{\partial \alpha_{\mu\mu}^e}{\partial x_i^\alpha} \right)_0 \left( \frac{\partial G_{\nu\nu}^e}{\partial x_j^\beta} \right)_0 \quad (8)$$

$$V(\beta_G^2)_{ai\beta j} = \frac{1}{2} \sum_{\mu,\nu} \left[ 3 \left( \frac{\partial \alpha_{\mu\nu}^e}{\partial x_i^\alpha} \right)_0 \left( \frac{\partial G_{\mu\nu}^e}{\partial x_j^\beta} \right)_0 - \left( \frac{\partial \alpha_{\mu\mu}^e}{\partial x_i^\alpha} \right)_0 \left( \frac{\partial G_{\nu\nu}^e}{\partial x_j^\beta} \right)_0 \right] \quad (9)$$

The index ‘0’ indicates that the derivatives are to be taken at the nuclear-equilibrium position.

**Computational Details.** – The tensors of *Eqns. 8* and *9* were computed with *HF* linear-response theory [20] by means of the DALTON program [21]. This approach has the advantage that the values of the molecular tensors are calculated for the frequency of the exciting laser light, in our case 532 nm, rather than for static electric and magnetic fields applied to a molecule. This matters, because the frequency dependence of the various tensor invariants, which appear in *Eqns. 1–3*, is not necessarily the same. For ROA, in particular, the invariants  $aG'$ ,  $\beta_G^2$ , and  $\beta_A^2$  can individually have the same or a different sign, and they also are combined with differing signs in the linear combinations appearing in *Eqns. 2* and *3*. The sign and size of computed ROA bands, therefore, depends on the subtle balance of the various invariants.

The *Cartesian* displacement vectors  $\mathbf{L}_{\alpha,p}^x$  of the nuclei  $\alpha$  in *Eqn. 6* were calculated with the DALTON program, but the force field and the molecular geometry was actually computed with DFT and the B3LYP hybrid functional [22] in GAUSSIAN [23]. The force field was transferred from GAUSSIAN to DALTON with a routine supplied with DALTON, which had been originally developed in our laboratory [24]. The reason for this somewhat cumbersome way of doing things is that Version 1.1 of DALTON does not include DFT.

The different basis sets used are indicated in the context of the discussion of the computed results. The basis set rDPS [8] is a non-standard set we developed for the computation of the electronic tensor part of *Raman* and ROA calculations. The acronym ‘DPS’ stands for ‘Diffuse Shell and Polarization’ function, with ‘r’ for ‘reduced’, indicating that diffuse polarization functions were added only to H-atoms. The valence part of the set corresponds to 3-21G [25]. Extensive work has shown that this diminutive set yields quantitatively acceptable and qualitatively reliable results for H-atom-containing organic molecules. As it is far from a complete set, a decisive requirement for its successful use is a gauge-origin-independent implementation of the theoretical expressions in *Eqns. 8* and *9*, which contain contractions of the optical-activity tensor  $G'$  with the electric-dipole/electric-dipole polarizability tensor. The use of a distributed gauge origin, as implemented in DALTON through the use of *London* orbitals [26], satisfies this condition.

**Representation of Vibrational Motion, Atomic-Contribution Pattern, and Group-Coupling Matrices.** – The graphical representation of vibrational motion in nonplanar polyatomic molecules, or even of out-of-plane motion in planar ones, has, in the past, been a major headache – one might simply look at attempts to represent such motion in classical works on vibrational spectroscopy [27][28]. An effective solution [3][18], applicable also to polyatomic chiral molecules, consists in graphically separating the size of the motion of a nucleus from the direction of the motion. The size, an isotropic quantity, can be represented by a sphere centered on a nucleus. The representation of  $|\mathbf{L}_{a,p}^x|$ , the magnitude of the excursion of a nucleus from the equilibrium position, is then independent of the orientation chosen for drawing the molecule. The direction of motion can be conveniently added by the appropriate shading of the spheres.

There are a number of options for choosing the size of a sphere. In the context of *Raman* and ROA spectroscopy, one might want to indicate the importance nuclear motion has in the formulae of *Raman*- and ROA-scattering cross-sections. With cross-sections representing areas, and nuclear excursions entering the formulae as the square, it is meaningful to draw the spheres with a diameter proportional to  $|\mathbf{L}_{a,p}^x|/\sqrt{\Delta\tilde{\nu}_p}$  [18], where the division by  $\sqrt{\Delta\tilde{\nu}_p}$  takes care of the decreasing importance nuclear motion has in *Raman* and ROA scattering with increasing vibrational frequency. The surface of the spheres is then a measure for the importance nuclear motion has in scattering cross-sections, and, thus, in generating *Raman* and ROA intensities.

The contribution of nuclear motion in scattering cross-sections is not the only possible criterion to choose the size of the spheres. If the primary goal of a graphical representation is to actually characterize vibrational modes, then the small physical motion of heavy atoms in most vibrations, as compared to that of H-atoms, makes it preferable to use mass-weighted coordinates.  $\mathbf{L}_{a,p}^x$  is then replaced by:

$$\mathbf{L}_{a,p} = \sqrt{m_a} \mathbf{L}_{a,p}^x \quad (10)$$

Such a graphical representation does not have an obvious geometrical interpretation. As  $|\mathbf{L}_{a,p}|^2$  is proportional to the kinetic energy of nucleus  $a$  in vibrational mode  $p$ , which is a scalar quantity, it appears best to choose the volume of the spheres, rather than their surface, proportional to  $|\mathbf{L}_{a,p}|^2$ .

Visualizing vibrational motion is useful for correlating vibrational modes in different molecules with similar structural elements, but knowing the shape of vibrational motion provides very limited insight only into how *Raman* and ROA intensities are generated. The two visualization tools, atomic-contribution pattern (ACP) and group-coupling matrices (GCM), have been developed, precisely with this problem in mind, in order to fill the need for a pictorial representation of how *Raman* and ROA intensities come about in a vibrating molecule [18]. While a detailed discussion exceeds the frame of the present work, the information conveyed by the two measures is readily explainable. The ACPs, on one hand, indicate the contribution each atom makes to the calculated *Raman* and ROA intensity, by the gradients of the relevant electronic tensors with respect to nuclear motion, and by the motion of the atomic nucleus, in a particular vibrational mode. In the GCMs, on the other hand, the diagonal elements indicate the contributions that groups of atoms make to *Raman* and

ROA scattering, with off-diagonal elements representing contributions due to the relative motion of the nuclei of the two different groups. Instead of figures arranged in two-dimensional arrays, we represent such contributions in general by the surface of circles.

**Geometry and Conformational Equilibria of the (4*S*)-4-Methylisochromane Moiety.** – (4*S*)-4-Methylisochromane ((4*S*)-**1**) exists in two major conformers that differ slightly in computed energy. In the more-stable conformation, the Me group at C(4) assumes a *pseudo*-axial and, in the less-stable one, a *pseudo*-equatorial position, respectively. Calculated with DFT, the B3LYP hybrid functional, and the 6-311G\*\* basis set [29], the ratio of the two conformers in the gas phase is 78:22 at 25°. A calculation with the smaller basis set 6-31G\* [30] yields the same ratio. In both conformations, the dihydropyran ring adopts a half-chair conformation, with the O-atom at the same side of the plane of the aromatic ring as the Me group in the *pseudo*-axial, and, at the opposite side, in the *pseudo*-equatorial conformation, respectively. The two C-atoms attached to the benzene ring lie essentially in its plane for both conformers, as shown in *Fig. 1* and in the *Table*.

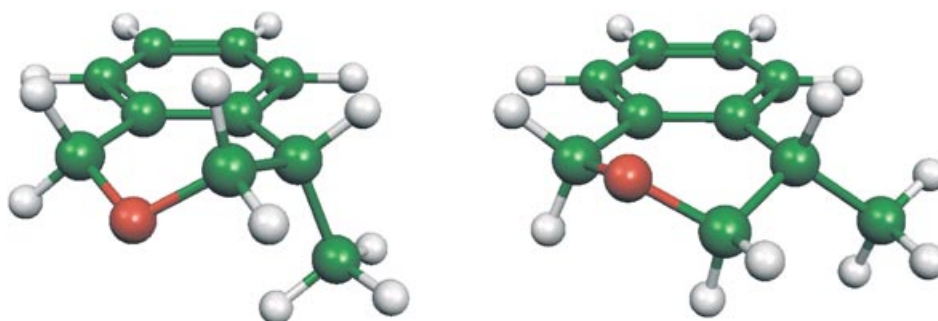
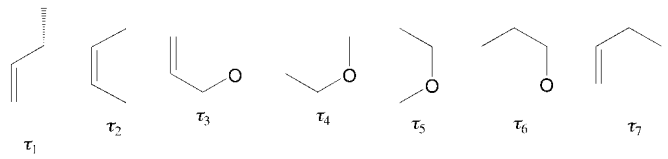


*Fig. 1. Computed geometry of the pseudo-axial (left) and the pseudo-equatorial (right) conformers of (4S)-4-methylisochromane (4S)-1*

We have added to the dihedral angles of the pyran ring of **1** those of the dihedral angles of the two (4*S*)-isomers<sup>2</sup>) of *Galaxolide*<sup>®</sup> (**2**), with the (7*R*)- and (7*S*)-configuration, respectively, as calculated with the 6-31G\* basis set (*Table*). The dihedral angles do not differ significantly for the two epimers, and they do not differ significantly from the values calculated for (4*S*)-**1** with either the 6-31G\* or the larger 6-311G\*\* basis set. It, therefore, appears that the unavoidable use of the relatively small 6-31G\* basis set for the calculation of the geometry of the (4*S*)-isomers of **2** does not represent a major limitation, and it moreover appears safe to conclude that neither the cyclopentene moiety, with its five attached Me groups, nor the absolute configuration at C(7) has a major influence on the structure of the dihydropyran ring of *Galaxolide*<sup>®</sup>.

The comparison of measured (*Fig. 2*) vs. computed (*Fig. 3*) *Raman* and ROA spectra can give independent confirmation of the presence of the *pseudo*-axial and the *pseudo*-equatorial form of (4*S*)-**1** in the condensed phase at room temperature. From

Table. Computed Dihedral Angles  $\tau$  ( $^\circ$ ) for the Two Conformational Minima of the Dihydropyran Ring of (4*S*)-**1**, (4*S*,7*R*)-**2**, and (4*S*,7*S*)-**2**. DFT with B3LYP functional, basis sets as indicated in the headings.



Configuration	Angle	(4 <i>S</i> )- <b>1</b>		(4 <i>S</i> ,7 <i>R</i> )- <b>2</b>	(4 <i>S</i> ,7 <i>S</i> )- <b>2</b>
		6-311G**	6-31G*	6-31G*	6-31G*
$\psi$ -ax	$\tau_1$	102.7	102.6	102.8	102.7
	$\tau_2$	2.3	2.7	2.5	2.5
	$\tau_3$	-14.8	-15.3	-15.3	-15.1
	$\tau_4$	48.0	48.3	48.4	48.3
	$\tau_5$	-69.1	-69.1	-69.2	-69.2
	$\tau_6$	52.7	52.6	52.6	52.7
	$\tau_7$	-20.4	-20.4	-20.3	-20.4
$\psi$ -eq	$\tau_1$	139.7	139.9	140.2	140.3
	$\tau_2$	-1.0	-1.0	-1.4	-1.4
	$\tau_3$	17.4	17.7	17.5	17.5
	$\tau_4$	-50.7	-50.9	-50.7	-50.6
	$\tau_5$	68.5	68.7	68.7	68.7
	$\tau_6$	-48.5	-48.8	-49.1	-49.2
	$\tau_7$	15.8	16.0	16.4	16.4

the calculated data, one finds that some *Raman* bands of the two conformers should be separately identifiable in the measured spectra. The two regions where this is most readily possible extend from 550 to 700  $\text{cm}^{-1}$ , and from 850 to 950  $\text{cm}^{-1}$ , and are indicated in the calculated spectra (Fig. 3). The vibrations leading to *Raman* bands distinguishable for the two conformers are the modes 13 (separately identifiable for the *pseudo*-axial and *pseudo*-equatorial form), 14 (*pseudo*-equatorial), and 20 and 21 (both *pseudo*-axial). Vibrations 20 and 21 also lead to prominent ROA signals for the *pseudo*-axial conformer, which are easily distinguishable in the measured spectrum, while 13 gives a ROA signal that allows the easy identification of the *pseudo*-equatorial form of **1**.

From the calculated spectra in Fig. 3, it is evident that the ROA spectra of the two conformers are far more different than is the case for the *Raman* spectra. This confirms the extreme sensitivity of ROA spectra to structural detail. Even where ROA bands show identical signs in both conformers, the sizes of the bands are generally different.

It is obvious that the experimental *Raman* and ROA spectra can be accounted for only by superposing spectra of individual conformers in an appropriate proportion. Moreover, the coefficients in the linear combination of the two spectra, yielding the theoretical spectrum in best overall agreement with the observed one, should give a good indication of the ratio in which the conformers are actually present in the condensed phase, as one expects *Raman* and ROA intensities to be similarly affected for the two conformers when one passes from the gas to the condensed phase.



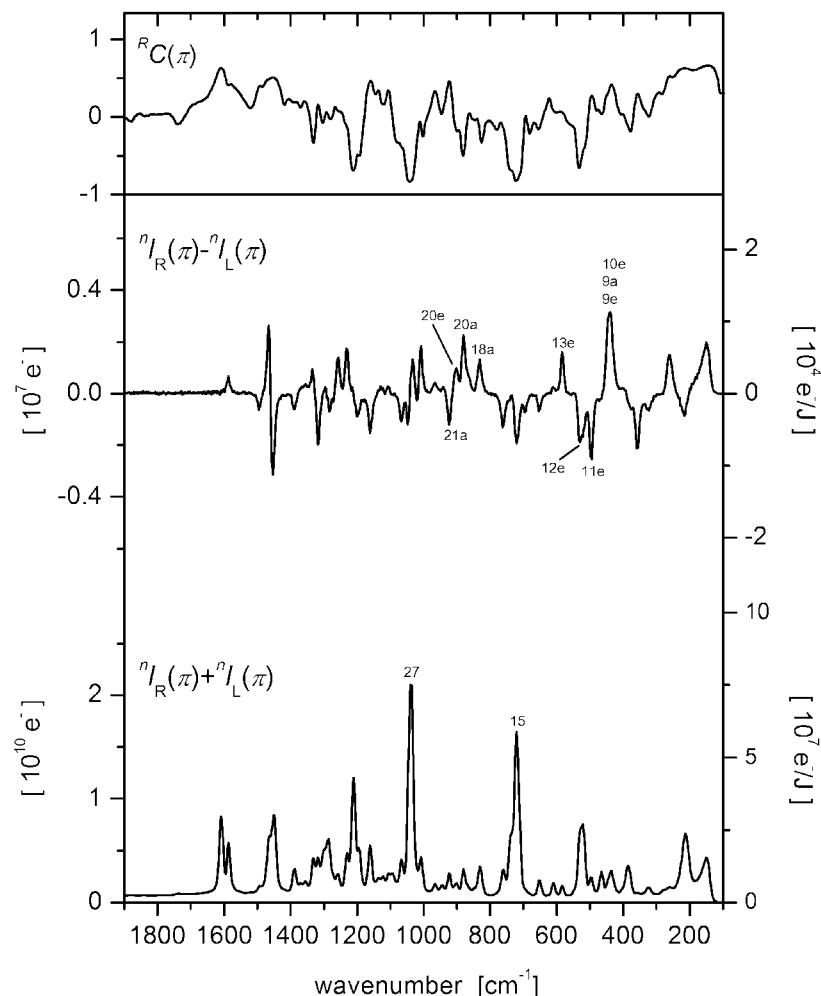


Fig. 2. Experimental room-temperature back-scattering Raman (bottom) and ROA spectra (middle) of (4S)-1, measured in the scattered-circular-polarization (SCP) mode. Letters *a* and *e* refer to the *pseudo*-axial and *pseudo*-equatorial conformers, respectively. On top, the degree of circularity is shown. It represents a measure of the polarization of the Raman bands and is not an expression of the chirality of the molecule (see text). Exposure time, 32.6 min; laser power at sample, 143 mW; exciting wavelength, 532 nm; resolution, 7 cm<sup>-1</sup>; sample size, 28 μl. The curves were slightly smoothed with the third-order five-point Savitzky–Golay procedure and represent detected electrons per CCD column, with one column covering *ca.* 2.4 cm<sup>-1</sup>.

In Fig. 4, theoretical Raman and ROA spectra for two differently weighted conformational mixtures are compared with the experimental spectra. They were generated by superposing the computed spectra of the *pseudo*-axial and the *pseudo*-equatorial forms in the abundance ratio 78:22, as calculated for the gas-phase, and, somewhat arbitrarily, in a 50:50 ratio. Both the Raman and the ROA spectra with the 50:50 ratio are in clearly better overall agreement with the measured spectra than the

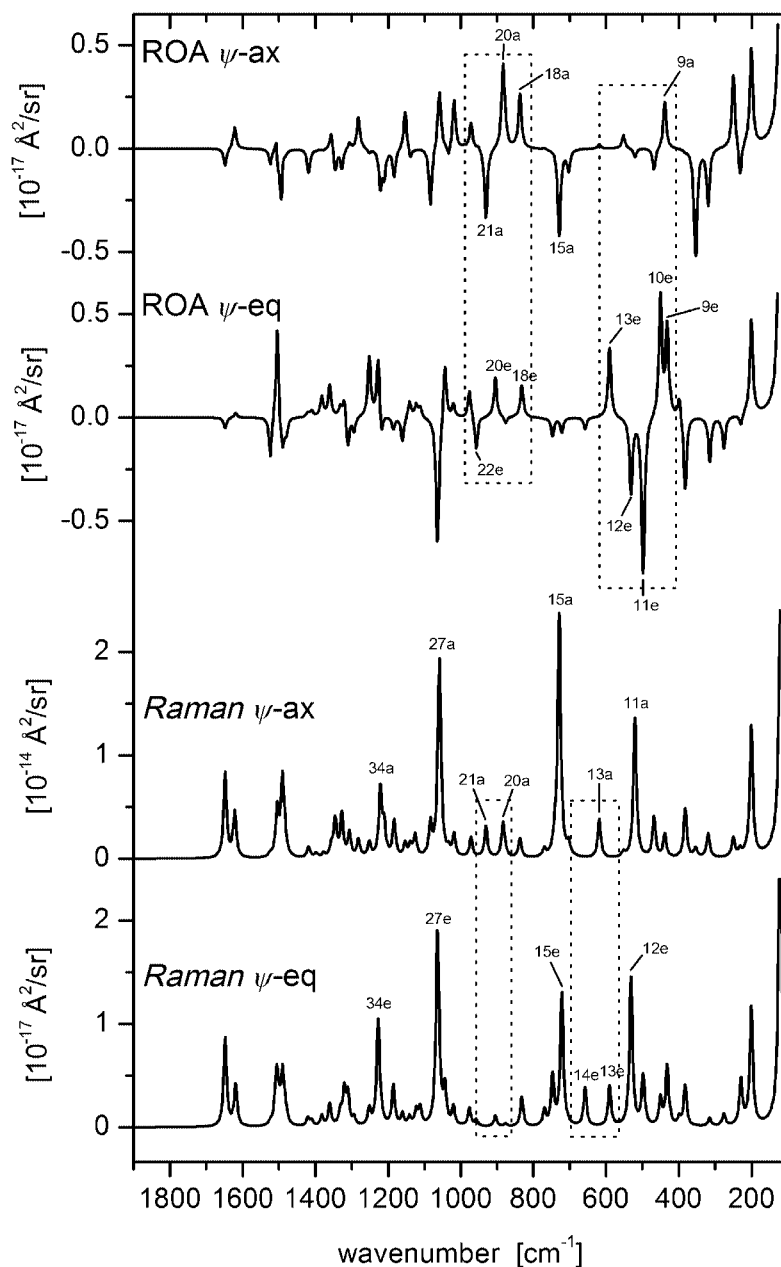


Fig. 3. Computed back-scattering Raman (lower part) and ROA spectra (upper part) of the pseudo-axial and pseudo-equatorial conformers of (4S)-1. The marked zones indicate spectral areas where individual bands for the two conformers can be separately identified. A Lorentzian band-shape with a full-width of  $10\text{ cm}^{-1}$  at half-maximum height was used. Geometry and vibrational modes, DFT with B3LYP and the 6-311G\*\* basis set; electronic tensors, *HF* linear-response theory with the rDPS basis set; exciting wavelength, 532 nm. The frequencies and the shapes of the vibrational modes were calculated in the harmonic approximation.

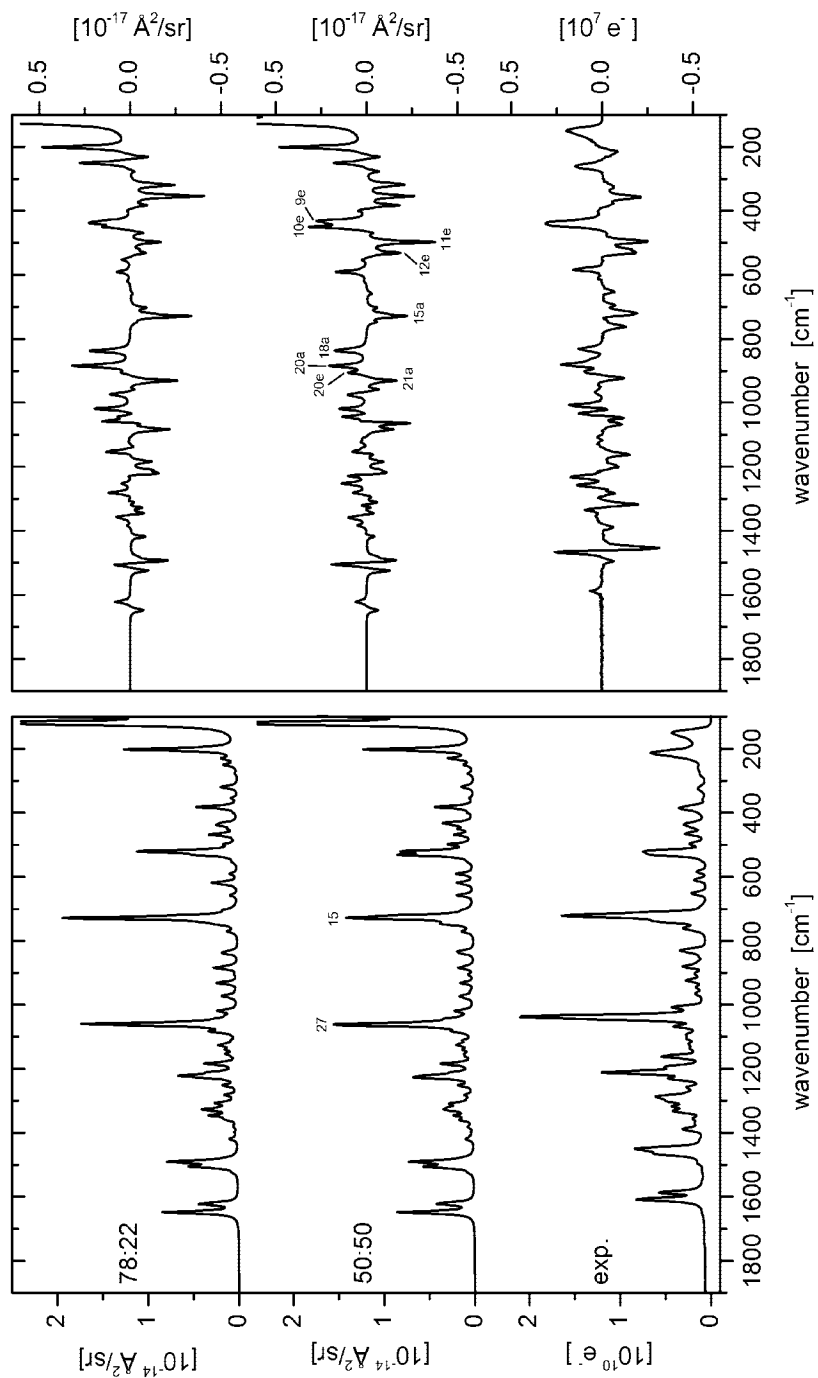


Fig. 4. Comparison of the experimental (bottom) and the synthetic (middle and top) Raman (left) and ROA (right) back-scattering spectra for the conformational mixtures pseudo-axial/pseudo-equatorial 78:22 and 50:50 of (4S)-1. The computational parameters are as in Fig. 3.

spectra obtained for the 78:22 ratio. It, therefore, appears that either the calculated gas-phase ratio of 78:22 is shifted in favor of the *pseudo*-equatorial form upon passing from the gas phase to the condensed phase, or that the ratio calculated for the gas phase is not correct to start with. In view of the small computed energy difference of only 3.1 kJ/mol for the two conformers, this latter possibility cannot be discarded.

In the *Raman* spectrum, improvements in going from a 78:22 to a 50:50 ratio are particularly visible from the relative size of the two dominant bands due to vibrations 15 and 27, from the better rendering of the shoulder at the high-wavenumber side of the band due to vibration 15, and from the bands due to vibrations 13 and 14 in the 550- to 700-cm<sup>-1</sup> region.

In the ROA spectrum, there are numerous details that improve upon going from a 78:22 to a 50:50 ratio. For the two spectral regions marked in *Fig. 4*, this is particularly visible, because ROA signals are dominated separately by the *pseudo*-equatorial conformer (450- to 600-cm<sup>-1</sup>) and the *pseudo*-axial conformer (810- to 930-cm<sup>-1</sup>). By simply adjusting the relative sizes of the spectral features of these two regions in the ‘synthetic’ spectrum to correspond to the relative size in the observed one, an abundance ratio of approximately 50:50 is again obtained for the two conformers.

We think that the comparison of ROA-signal intensities of the two specified regions is a reasonable approach to semi-quantitatively assess the relative abundance of the two conformers, because the calculated ROA signals of the vibrations 9 to 13, which dominate the 450- to 600-cm<sup>-1</sup> region, are large, the largest ones calculated for the *pseudo*-equatorial conformer, with the same holding true for the ROA signals of vibrations 20 and 21 in the 810- to 930-cm<sup>-1</sup> region for the *pseudo*-axial conformer. The relative size of such large ROA effects is generally well reproduced by the level of theory used here, as has been demonstrated for the calculated ROA spectrum of the rigid molecule (–)-(M)-σ-[4]helicene by means of a computational approach essentially identical to the one used in the present work [6].

**Interpretation of Spectral Features, and the Absolute Configuration at C(4).** – *Raman Spectra.* The two most-prominent bands in the *Raman* spectrum of (4*S*)-4-methylisochromane ((4*S*)-**1**) are due to vibrations 15 and 27 (*Figs. 2* and *3*), and are fairly polarized. As is often the case for such bands, they have small  $\Delta$ -values, with  $\Delta$  corresponding to the ratio of the ROA to the *Raman* intensity.

The polarization of the bands can be inferred from the degree of circularity  ${}^RC(\pi)$  measured in back-scattering, which has been included in *Fig. 2*. The reason for presenting the degree of circularity rather than the better-known depolarization ratio  $\rho_{\perp}$  is that the former can be easily measured with our SCP-ROA instrument [31][32] without changing optics. The depolarization ratio  $\rho_{\perp}$  can then be calculated as follows [33]:

$$\rho_{\perp} = \frac{1 + {}^RC(\pi)}{3 - {}^RC(\pi)} \quad (11)$$

The value  ${}^RC(\pi) = -1$ , therefore, corresponds to a fully polarized *Raman* band with  $\rho_{\perp} = 0$ ,  ${}^RC(\pi) = 5/7$  corresponds to a completely depolarized band with  $\rho_{\perp} = 3/4$ , and  ${}^RC(\pi) = 0$  represents a moderately polarized band with  $\rho_{\perp} = 1/3$ .

The shape of the vibrations 15 and 27 of (4*S*)-**1** are depicted in Fig. 5. They are examples of vibrations that have a strong heritage from similar vibrations found in *ortho*-disubstituted benzenes. Their shapes are similar in the *pseudo*-axial and *pseudo*-equatorial forms of (4*S*)-**1**. As is typical for vibrations leading to polarized bands, they show some approximate symmetry with respect to local or global molecular-structural elements.

Vibration 15, which occurs at *ca.* 722 cm<sup>-1</sup>, is related to an in-plane vibration, which, in *ortho*-xylene (=1,2-dimethylbenzene), leads to the most-intense *Raman* band at 735 cm<sup>-1</sup> [27]. It can be traced back to the ring-deformation mode 6a (*Wilson* notation) in benzene. In nonplanar (4*S*)-**1**, this vibration acquires a substantial component from out-of-plane vibrations, which are found in *ortho*-xylene at a similar frequency.

Vibration 27 occurs at 1038 cm<sup>-1</sup>, and corresponds to vibration 18*b* in benzene. Its localization on the benzene moiety is even more pronounced than for vibration 15, and all nuclei of the benzene moiety move essentially in the plane of the aromatic ring. An intense polarized band due to a vibration with a similar shape is likewise found in *ortho*-xylene at almost the same frequency. From the strong localization of vibration 27, one expects its *Raman* atomic-contribution pattern (ACP) to be largely independent of the conformation of **1**; and, from Fig. 5, this is seen to be the case.

The fate of the two vibrations 15 and 27, upon going from (4*S*)-**1** to the (4*S*)-isomers of *Galaxolide*® (**2**), is not the same. As is obvious from its shape, vibration 27 cannot ‘survive’ substitution at C(6) and C(7) of the isochromane moiety, and, thus, no similar vibrational mode is found in (4*S*)-**2**. In contrast, vibration 15 leads to vibration 36 in (4*S*)-**2**. This vibration gives rise to two intense, polarized bands in the *Raman* spectrum, as seen in Fig. 6.

The appearance of two bands for vibration 36, one at a higher and the other at a lower frequency than the band of vibration 15 in (4*S*)-**1**, is puzzling at first sight, but it can readily be understood by looking at the shape and the *Raman* ACPs of vibration 36 in the two conformers of (4*S*)-*Galaxolide* (**2**) (Fig. 7). In the *pseudo*-axial conformer, the shape of vibration 36 is very similar, with a similar *Raman* ACP, to the shape of vibration 15 in (4*S*)-**1**, except that the vibration has a slightly higher energy. In the *pseudo*-equatorial conformer, the situation is different, and the original ring-deformation mode 6a of benzene no longer couples with the pyran ring, but rather with a deformation mode of the five-ring moiety. This leads to a composite vibration with a slightly lower energy than that of vibration 15, and with a *Raman* ACP that is different, except for the two central C- and H-atoms of the aromatic part of the molecule. These findings are independent of the absolute configuration at C(7) of **2** and, therefore, apply to both (4*S*,7*S*)- and (4*S*),7*R*)-**2**.

**ROA Spectra.** The understanding of the two marked regions extending from 450 to 600 cm<sup>-1</sup> and from 800 to 950 cm<sup>-1</sup> in the ROA spectrum of (4*S*)-**1** in Fig. 3 is of interest because the ROA signals of the two conformers are separately identifiable. A further region of stereochemical relevance extends from 1450 to 1550 cm<sup>-1</sup>, and reflects the coupling of the antisymmetric, doubly degenerate deformation mode of the Me group with vibrations 19*a* and 19*b* (*Wilson*) of the benzene ring [34]. It can equally well be exploited for assigning the absolute configuration at C(4) [35][36]. However, a detailed discussion of the many spectral features useful to this end exceeds the scope of the present work, and we will, thus, concentrate on vibration 20 of the 800- to 950-cm<sup>-1</sup>

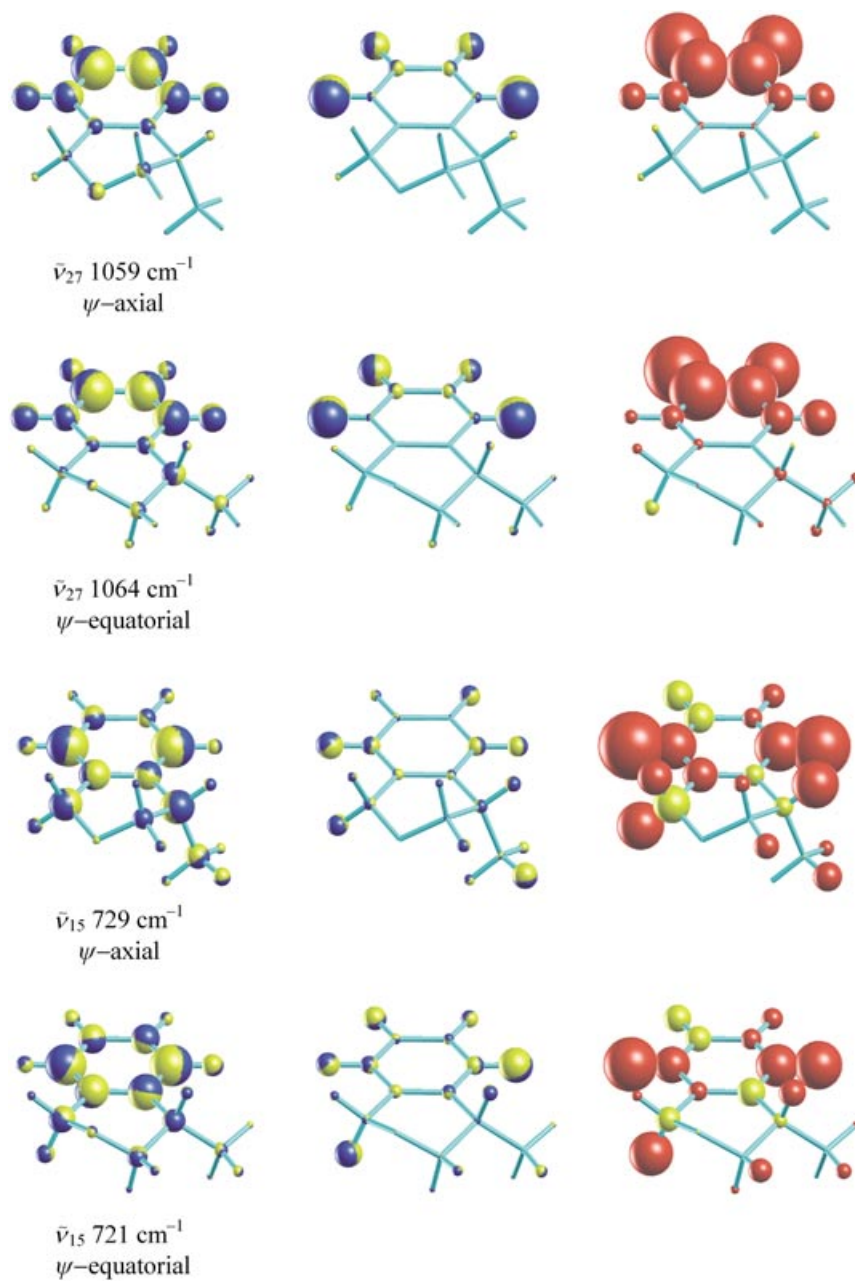


Fig. 5. Vibrational modes 15 and 27 responsible for the dominant Raman bands at 722 and 1038  $\text{cm}^{-1}$  in the experimental spectrum of (4S)-**1** (see Fig. 2). The bands are not separately identifiable for the two conformers. Left column, vibrational-energy distribution; middle column, shape of vibrational modes; right column, Raman atomic-contribution pattern (Raman-ACP). For computational details, see text.

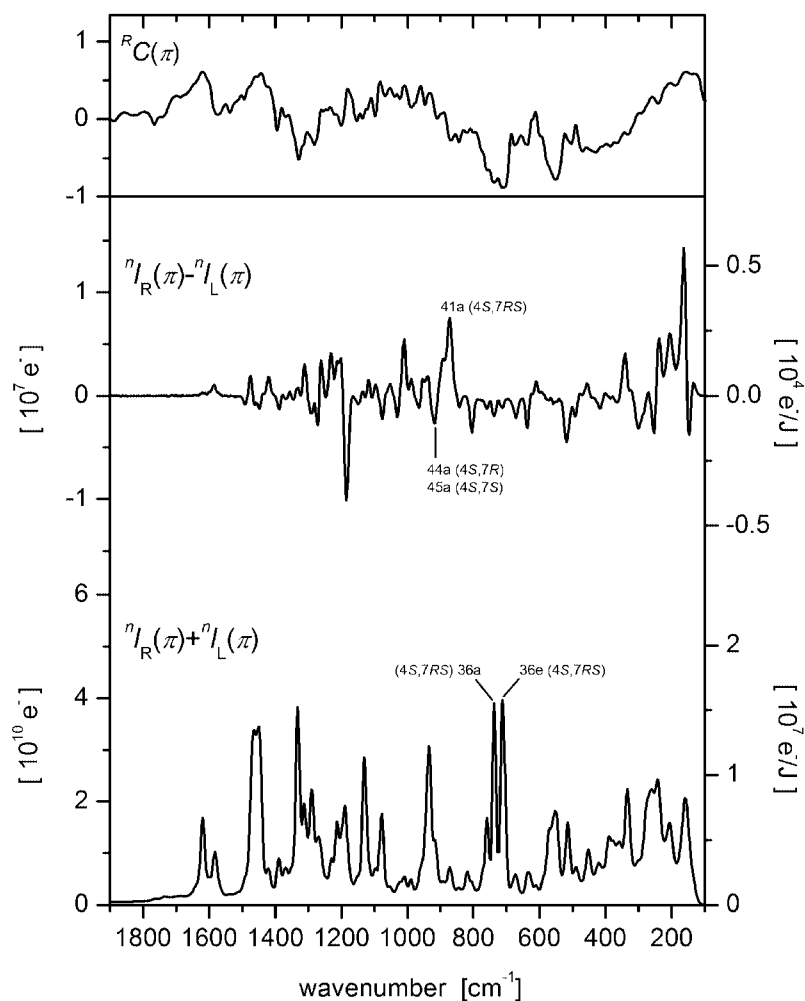


Fig. 6. Experimental room-temperature back-scattering Raman (bottom) and ROA spectra (middle) of diastereoisomeric mixture of (4S,7R)-**2** and (4S,7S)-**2**, measured in the scattered-circular polarization (SCP) mode. On top, the degree of circularity is shown. Exposure time, 52.7 min; laser power at sample, 810 mW; sample size, 35  $\mu$ l. For other parameters, see Fig. 2.

region. The comparison with vibration 41 of (4S)-**2**, for the *pseudo*-axial conformer, yields a particularly solid argument for assigning the absolute configuration at C(4) independently of that at C(7).

The shapes and the ROA ACPs of vibrations 20 of (4S)-**1** and 41 of (4S)-**2**, respectively, are shown in Fig. 8 for the *pseudo*-axial conformation. The nuclei that move by far the most in both vibrations belong to three H-atoms, one attached to the stereogenic center C(4), the other two attached to adjacent C-atoms. Despite the similarity and the localization of these vibrations, the ROA ACPs are different for **1**

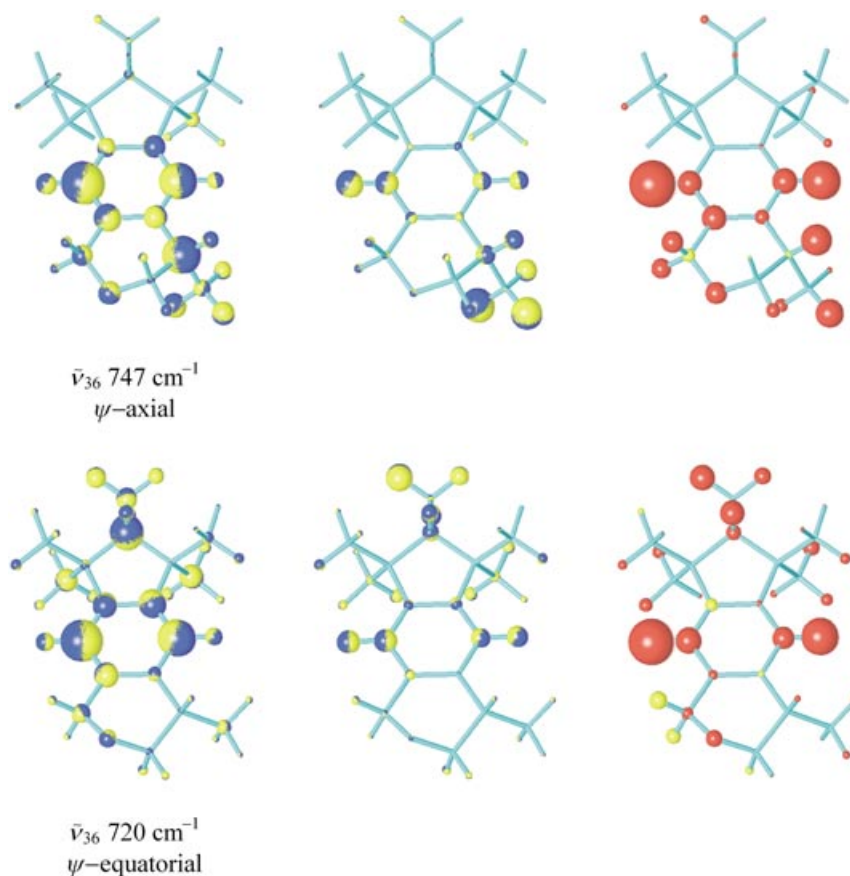


Fig. 7. Vibrational mode 36 responsible for the two dominant Raman peaks at 737 and 713  $\text{cm}^{-1}$  in the experimental spectrum of the diastereoisomeric mixture of (4*S*,7*R*)- and (4*S*,7*S*)-**2** (see Fig. 6). The peaks correspond to the *pseudo*-axial and the *pseudo*-equatorial conformers, as indicated, irrespective of the diastereoisomer. Left column, vibrational-energy distribution; middle column, shape of vibrational modes; right column, *Raman*-ACP. For computational details, see text.

and **2**, but are essentially identical for (4*S*,7*R*)-**2** and (4*S*,7*S*)-**2**. The much larger ROA ACPs of the (4*S*)-diastereoisomers of *Galaxolide*<sup>®</sup> come about by coupling terms between the three H-atoms, with the largest excursions of the substituted pyran moiety and the atoms of the methylated cyclopentene moiety. This is born out by the group-coupling matrices shown in Fig. 9.

The observation of such a long-distance coupling, and of its effect on ROA ACPs, is important because it questions the generally hold idea that nonresonant ROA is inherently a short-range effect [37][38]. We have verified, as far as possible, that our observation is not due to an artifact produced by the small basis sets used in the calculation of the (4*S*)-isomers of *Galaxolide*<sup>®</sup>. This does not, indeed, seem to be the case as, for (4*S*)-4-methylisochromane (4*S*)-**1** and vibration 20, the small sets reproduce



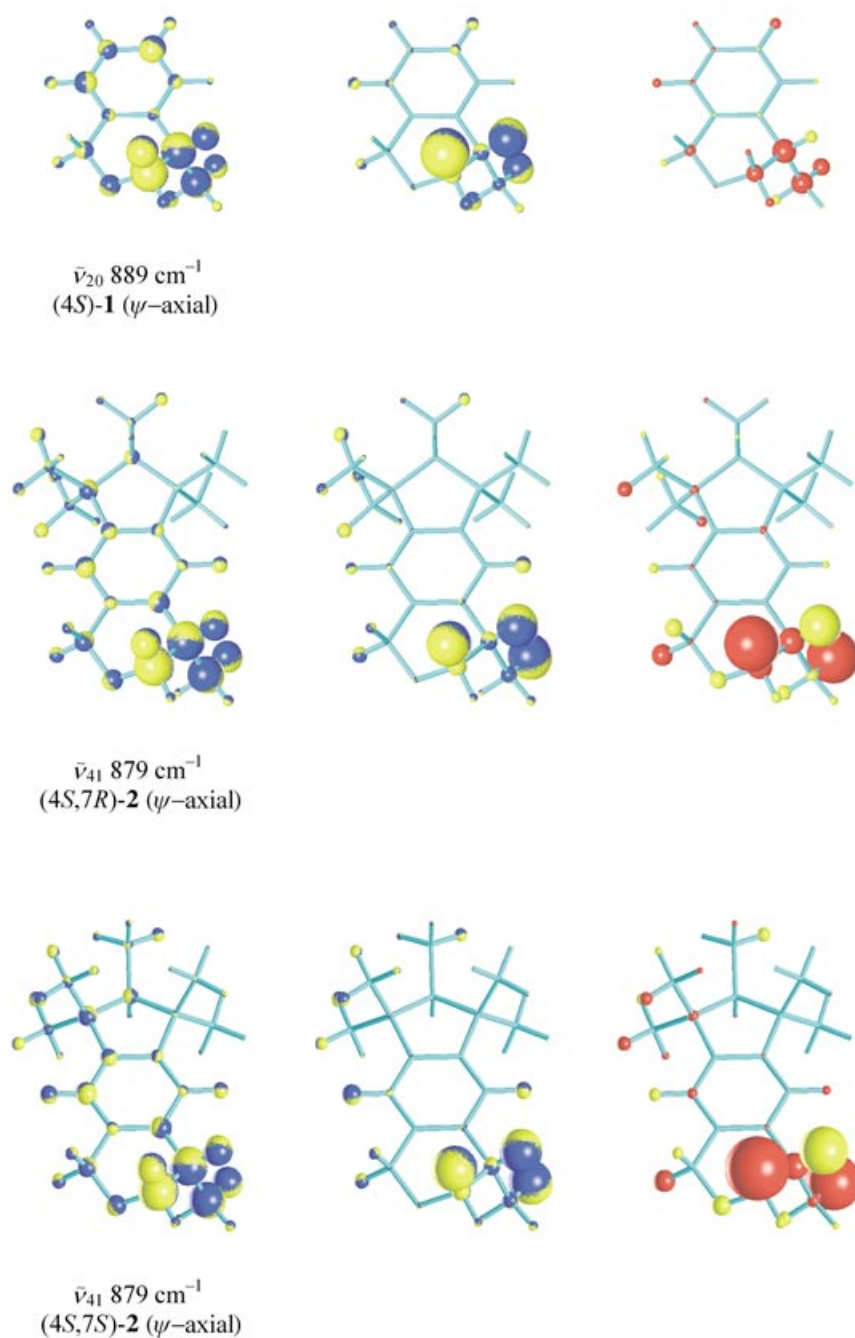


Fig. 8. Comparison of vibrational mode 41 of (4*S*,7*R*)- and (4*S*,7*S*)-**2** with vibrational mode 20 of (4*S*)-**1** for the *pseudo*-axial conformers. The two vibrations sample predominantly the absolute configuration at C(4). Left column, vibrational-energy distribution; middle column, shape of vibrational modes; right column, ROA-ACP. The basis sets used for (4*S*)-**2** are smaller than those for (4*S*)-**1**, but the graphical representations obtained with the smaller sets for the latter agree with those given here for the larger sets.

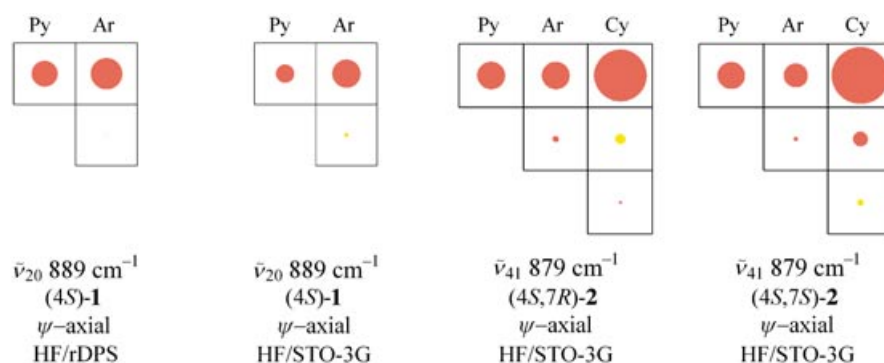


Fig. 9. Comparison of the group-coupling matrix (GCM) of vibration 41 of (4S,7R)- and (4S,7S)-2 (right-hand side) with that of vibration 20 of (4S)-1 (left-hand side). Ar, benzene rings; Py, substituted dihydropyran rings (except for C-atoms in common with the benzene ring); Cy, methylated cyclopentene moiety (except for C-atoms in common with the benzene ring). Most of the ROA of vibration 41 comes about by long-range coupling of the Py and Cy moieties.

the ROA ACPs of larger sets reasonably well. Moreover, the experimental data of Figs. 2 and 6 also lend support to our conclusion.

In the *pseudo*-equatorial form of the molecules, the aspect of vibrations 20 and 41 changes completely, and both are shifted to higher energies. The band due to vibration 20 of the *pseudo*-equatorial form of (4S)-1 can readily be identified in the experimental spectrum of Fig. 2. The shift to higher energy of vibration 41 for the *pseudo*-equatorial conformers of (4S)-2 reflects the fact that it is now related to the higher-energy vibration 21 of the *pseudo*-equatorial conformer of (4S)-1.

**Calculated Spectra and Absolute Configuration at C(7) of the (4S)-Isomers of Galaxolide®.** – *Back-Scattering Spectra.* In the last section, for determining the absolute configuration at C(4), the ROA vibrations of interest were those that proved sensitive to the absolute configuration at C(4) but insensitive to that at C(7). Now, we are interested in vibrations of opposite behavior, *i.e.*, sensitivity to the absolute configuration at C(7), but insensitivity to that at C(4). An interesting difference, and a test of the potential of ROA, follows from the locally achiral environment of C(7). It is only by the presence of the substituted pyran ring that C(7) becomes stereogenic. At first sight, it, therefore, appears more difficult to find vibrations primarily reflecting the configuration at C(7) than to find vibrations useful for determining the configuration at C(4).

We have shown elsewhere that chirality due to electron distribution is, in general, of lesser importance for the ROA than chirality due to vibrational modes [3]. Promising candidates for vibrations sampling the absolute configuration at C(7), therefore, have to extend over the cyclopentene as well as the pyran moiety, as the slight electronic asymmetry induced into the methylated cyclopentene moiety by the presence of the pyran ring will not lead to substantial ROA. On the other hand, for a vibration to reflect the absolute configuration of C(7) rather than C(4), it will need to have its main component on the methylated cyclopentene moiety, with only a minor, but distinct, component on the pyran ring. This is the precise opposite of what we found for vibration 41 used for determining the absolute configuration at C(4).

In *Fig. 10*, we present the three vibrations 44, 45, and 46 of the *pseudo*-axial form of (4*S*)-**2**, which all satisfy the above criteria. The shape of their minor component on the pyran moiety is clearly related, for all three modes, to vibration 21 of (4*S*)-**1**, as also shown in *Fig. 10*. Vibration 21 has, therefore, the character of a large-scale group vibration, similar to the slightly more-localized vibration 20 discussed for the substituted *pseudo*-axial pyran ring in the previous section. While the persistence of large-scale group vibrations in highly symmetric vibrational chromophores that are part of larger molecules is well known, the same phenomenon for large, nonsymmetric vibrational chromophores, such as, here, the substituted pyran moiety, does not seem to have been identified up to now.

Vibrations 45 and 46 are computed to occur within  $4\text{ cm}^{-1}$  of each other for all diastereoisomers and conformers of *Galaxolide*<sup>®</sup> (**2**). The two vibrations are, therefore, expected to lead to a single band in the experimental spectrum, and they certainly do so in the computed spectra shown in *Fig. 11*. According to our calculations, the two vibrations lead to ROAs of opposite sign but unequal size, with mode 45 always negative and mode 46 always positive. The relative size depends on the absolute configurations at C(4) and at C(7), and on the conformation of **2**, and the numbering of the bands refers to the vibration that yields the dominant ROA contribution. Thus, as seen from *Fig. 11*, while we do not have a sign change from positive to negative for vibrations 45 and 46 individually in going from (4*S*,7*R*) to (4*S*,7*S*), we expect a sign change for the ROA band that results from the combined ROA intensities of the two individual vibrations. As the experimental spectrum shown in *Fig. 6* has been recorded for the diastereoisomeric mixture (4*S*)-**2**<sup>2</sup>), and, as for this mixture the combined ROA of vibrations 45 and 46 essentially compensates, this computational prediction cannot be verified at present, but experimental verification should be possible in the foreseeable future<sup>3</sup>).

The computed ROA of vibration 44 follows more closely the ideal situation outlined above, where the ROA of a single vibration changes sign in going from (4*S*,7*R*)- to (4*S*,7*S*)-**2**. As the size of the negative ROA of vibration 44 is much larger for the (4*S*,7*R*)-diastereoisomer of **2** than the size of the positive ROA for the corresponding (4*S*,7*S*) diastereoisomer, the band due to vibration 44 can be readily identified in the experimental spectrum of the isomer mixture (*Fig. 6*).

For the (4*S*)-isomers of *Galaxolide*<sup>®</sup> (**2**), we had to rely on the shape of vibrations calculated by means of DFT (6-31G\* basis set), with ROA intensities calculated with *HF* and STO-3G. One might justifiably ask what physical significance one can attribute to results obtained with this slightly adventurous combination. In *Fig. 12*, at the danger of repeating the experimental ROA curves, we directly compare the ROA spectra computed with 6-31G\*/STO-3G with the experimental ones for (4*S*)-**1** and (4*S*)-**2**. A 50 : 50 mixture of the *pseudo*-axial and *pseudo*-equatorial conformers was chosen for the computed data. There are some obvious discrepancies, particularly at wavenumber shifts higher than *ca.*  $1100\text{ cm}^{-1}$ , but at lower wavenumbers, the qualitative agreement is generally acceptable. Clearly, where the primary goal is the prediction of the absolute configuration of a large chiral molecule, the 6-31G\*/STO-3G combination is a useful

<sup>3</sup>) Note added in proof: The recent measurement of the ROA spectrum of the (4*S*,7*R*)-isomer of *Galaxolide*<sup>®</sup> has confirmed the predictions made for vibrations 44, 45, and 46.

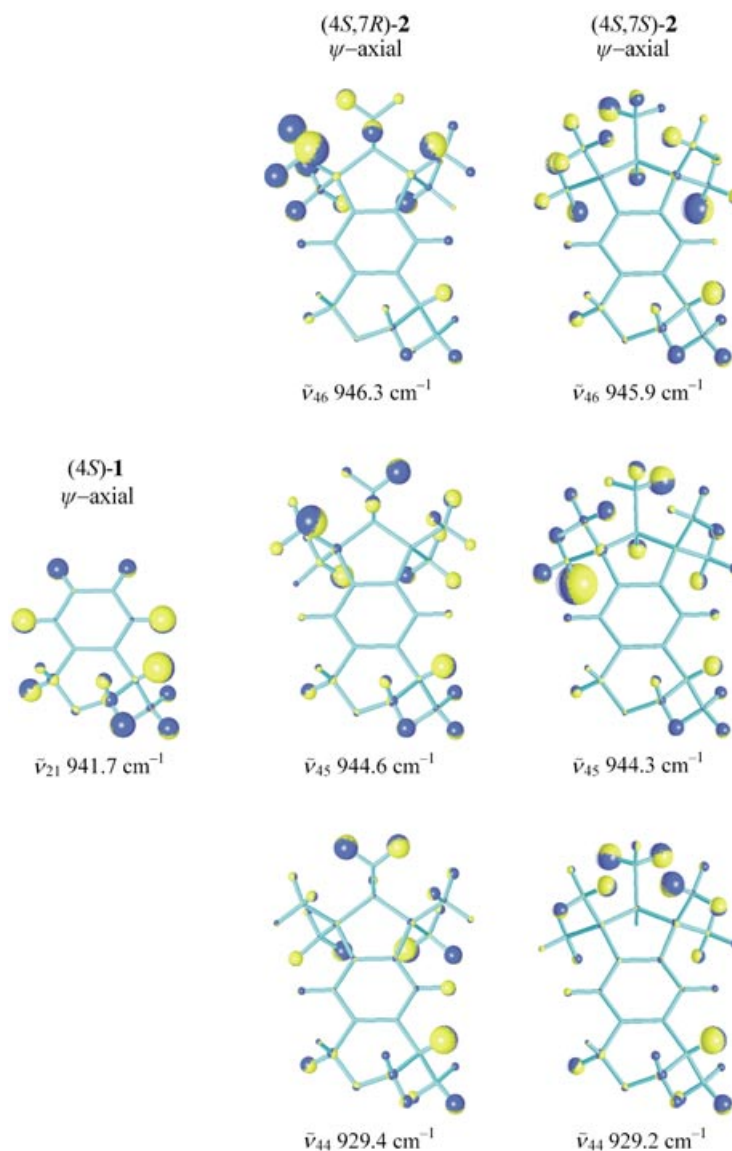


Fig. 10. *Shape of vibrations 44, 45, and 46*, which sample predominantly the absolute configuration at C(7). The ROA of vibration *44* changes its sign from negative to positive in going from (4*S*,7*R*)-**2** to (4*S*,7*S*)-**2**. Vibrations *45* and *46* do not individually change sign, but lead to a single ROA band that changes sign from positive to negative. Shown are the *pseudo*-axial conformers. In the *pseudo*-equatorial conformers (not shown), motion on the methylated cyclopentene moiety remains related to that of the *pseudo*-axial one.

approach. Two of the conditions not further discussed here, but verified by numerous calculations, are that DFT must be used for the vibrational part, and that the molecular skeleton should primarily be hydrocarbon in nature.

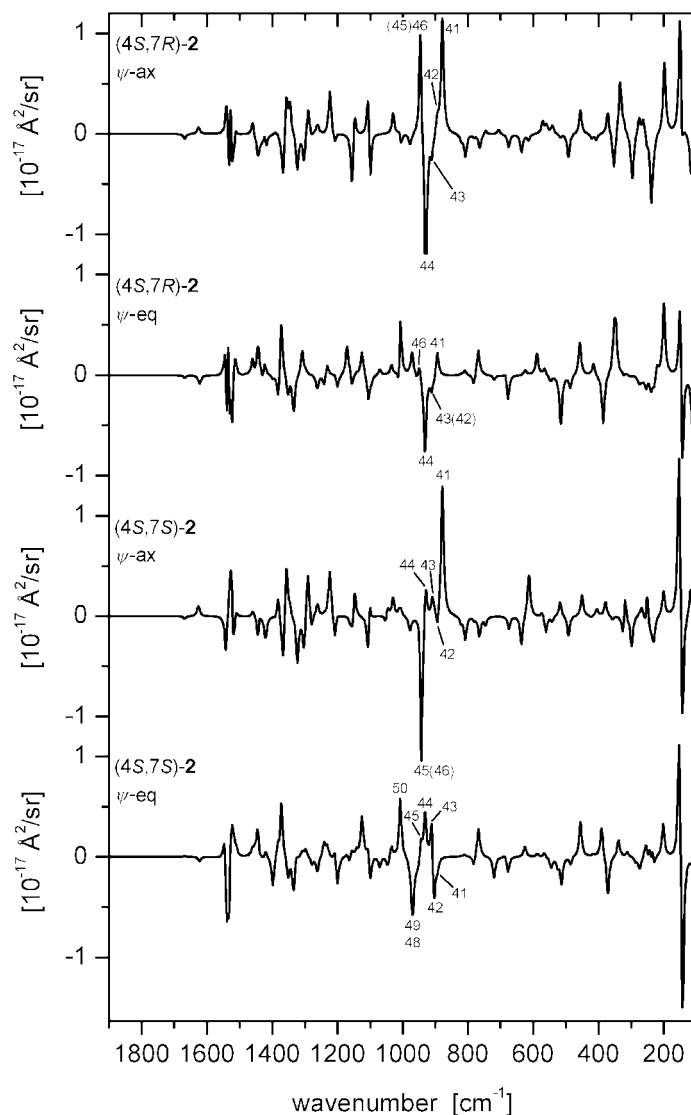


Fig. 11. Computed back-scattering ROA spectra of the pseudo-axial and the pseudo-equatorial conformers of the two diastereoisomers of (4S)-Galaxolide (**2**). Geometry and vibrational modes, DFT with B3LYP and the 6-31G\* basis set; electronic tensors, *HF* linear-response theory with the STO-3G basis set; for other parameters, see Fig. 3.

*The Potential of Forward-Scattering.* We have found [8] that ROA measured in forward-scattering [16] can, sometimes, more reliably be calculated than ROA in back-scattering. This was one of the reasons for also computing the forward-scattering spectra of (4S)-**2**, another being that a new instrument for measuring SCP ROA in forward-scattering is currently under construction in our laboratory. To our pleasant

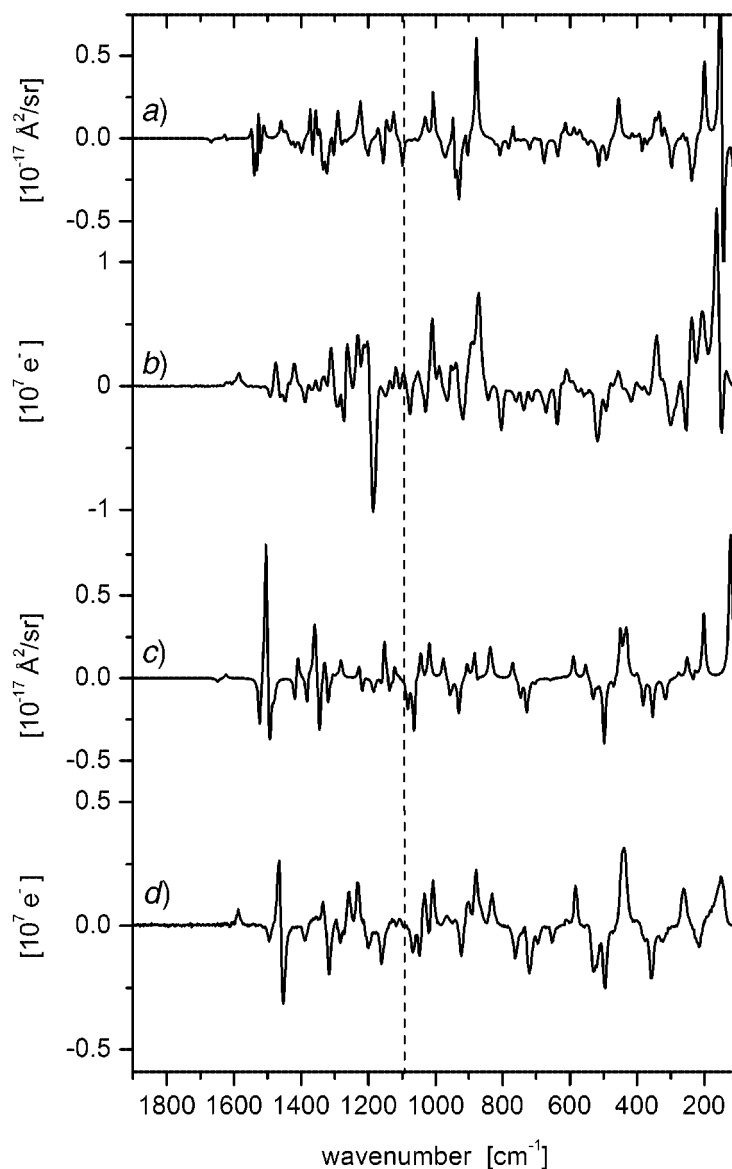


Fig. 12. Comparison of the synthetic (a) with the experimental (b) back-scattering ROA spectrum of a 50:50 diastereoisomeric mixture of (4S,7R)- and (4S,7S)-**2**. A 50:50 pseudo-axial/pseudo-equatorial conformation was assumed for a. The computational parameters are as in Fig. 11. Comparison of the synthetic (c) with the experimental (d) back-scattering ROA spectrum of (4S)-**1**, but for the HF/STO-3G//B3LYP/6-31G\* combination used in a. Quantitative agreement clearly suffers in comparison to Fig. 4, but general qualitative agreement between the computed and measured data is retained for wavenumber shifts lower than 1100  $\text{cm}^{-1}$  (dashed vertical line).

surprise, we found that the absolute configuration at C(7) should be easily identifiable in ROA forward-scattering.

The computed ROA spectra for forward-scattering of a 50:50 mixture of *pseudo*-axial and *pseudo*-equatorial conformers of (4*S*)-**2** are shown in Fig. 13. There are differences in the 750- to 850-cm<sup>-1</sup> spectral region, which can, once the experimental spectra of the two diastereoisomers will be available, almost certainly be exploited for assigning their absolute configurations at C(7) independently of that at C(4). The most-visible changes are found, however, in the vicinity of 250 cm<sup>-1</sup> for vibrations 12, 13, and 14. This spectral region is, generally, for fair-sized organic molecules, dominated by large-scale skeletal-deformation motions and by torsional modes of Me groups.

The spectral region is easily accessible with modern ROA instrumentation. What is, at present, less well known is what influence both anharmonicity and interactions in the condensed phase may have on the ROA of low-frequency vibrations. The sign of the very small ROA effect measured for the condensed phase in back-scattering for the pure torsional motion of the Me group in methyloxirane disagrees with the sign computed for the gas phase in the harmonic approximation [8][39]. However, the effects discussed here for the 250-cm<sup>-1</sup> spectral region are large relative to other spectral features in the forward-scattering spectra, and so, chances might be better for

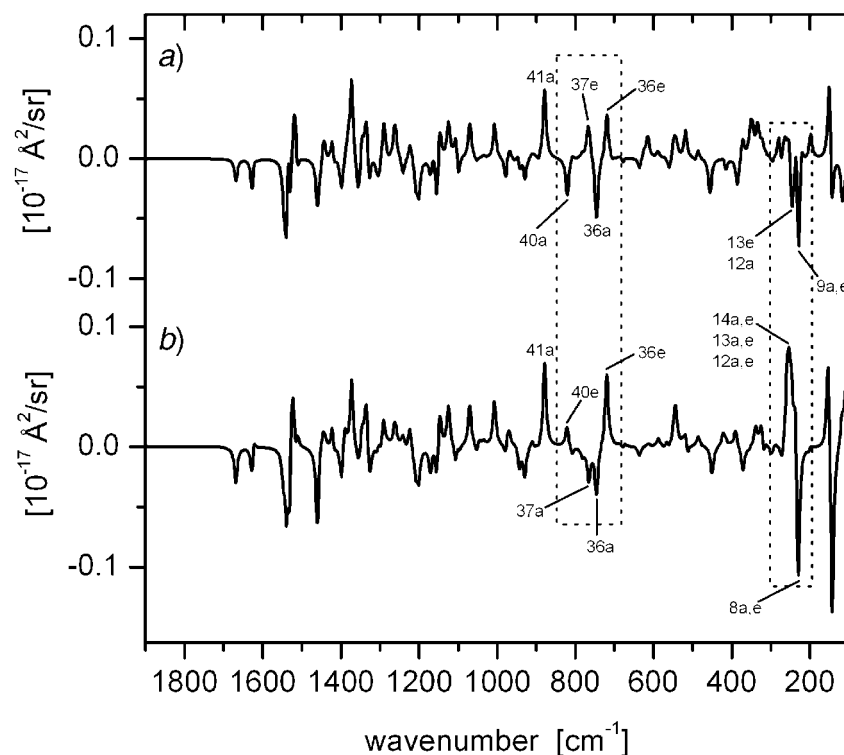


Fig. 13. Computed ROA forward-scattering spectra for (4*S*,7*R*)-**2** (a) and (4*S*,7*S*)-**2** (b). The two zones where the most-pronounced changes occur in going from the (7*R*)- to the (7*S*)-configuration are marked. For computational parameters, see Fig. 11.

computed and measured data to qualitatively agree. The availability of experimental data will eventually decide whether low-frequency ROA data measured in forward-scattering are useful or not.

The shapes of the vibrations *12*, *13*, and *14*, which cause the large positive ROA band at 254 cm<sup>-1</sup> characteristic for the (4*S*,7*S*)-configuration of **2**, is shown in *Fig. 14*. All three vibrations have a pronounced component of torsional motion at one or more of the Me substituents of the cyclopentane ring. In vibrations *12* and *14*, the dominant torsional motion rests with the Me group at C(7). The whole Me group, including the C-atom, also exerts a wagging-like motion from right to left with the molecule drawn as in *Fig. 14*, and the motion in space of the three H-atom nuclei, therefore, does not represent a pure torsional motion. This is even more the case for vibration *13*, where the same Me group exerts an up-and-down motion, combined with a minor torsional component only.

The group-coupling matrices in *Fig. 14* indicate that much of the ROA intensities of vibrations *12*, *13*, and *14* for (4*S*,7*S*)-**2** is due to the interaction of the methylated cyclopentane ring with the substituted pyran ring. This is to be expected in view of what has been stated in the previous section concerning the need for a vibration to extend over the whole molecule, in order to be able to sample the absolute configuration of **2** at C(7).

For the (4*S*,7*R*)-configuration, vibrations *12*, *13*, and *14* bear little resemblance with their counterparts for the (4*S*,7*S*)-configuration. The main similarity is that they are, again, composed of torsional motions of the six Me groups of **2**, combined with skeletal motions. Their group-coupling matrices show positive and negative contributions, with a value close to zero for the sum of the ROAs for the three vibrations.

**Conclusions.** – The (4*S*)-configuration of the olfactorily most-potent (4*S*,7*R*)- and (4*S*,7*S*)-isomers of *Galaxolide*® (**2**) was deduced by *Fráter et al.* [11], who synthesized these isomers *via Friedel–Crafts* coupling of pentamethylindane with (*S*)-propylene oxide, which is alkylated under inversion [40]. In the present work, we confirmed the absolute (4*S*)-configuration by *Raman*-optical-activity (ROA) spectroscopy.

In the recent past, the main area of application of ROA has been the investigation of the structure of biopolymers. One of the aims of the present study has been to demonstrate the potential the precision-measurement of ROA spectra [31][32] has, especially in conjunction with modern *ab initio* calculations, for the determination of absolute configurations and conformational equilibria of standard organic, chiral molecules such as *Galaxolide*® (**2**).

The study of *Galaxolide*® bears several aspects of particular interest. One is the separate availability of (4*S*)-4-methylisochromane (4*S*)-**1**, the major chiral molecular fragment of the (4*S*)-isomers<sup>2</sup> of *Galaxolide*®, which allowed us to demonstrate a correlation between the ROA spectra of the two molecules. Another is the *second* stereogenic center C(7) of **2**. This center is located in an essentially nonchiral local environment, sufficiently distant from C(4), so that, even with the absolute configuration at C(4) known, the absolute configuration at C(7) *cannot* be determined by NMR spectroscopy. A third important aspect is the presence of two conformers in comparable amounts. By successfully dealing with these complications, we have shown that ROA can give a clear-cut answer to the question of the absolute configuration of



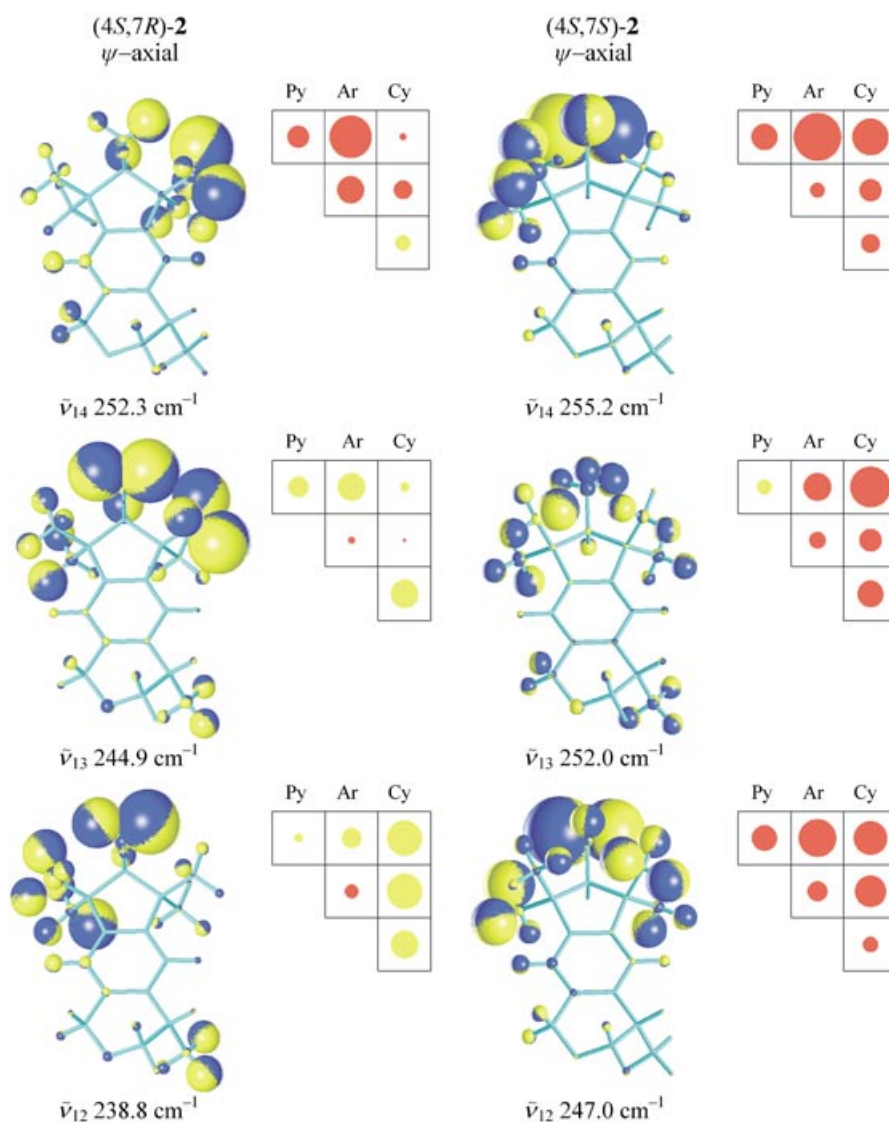


Fig. 14. Shape and group-coupling matrices of the vibrational modes 12, 13, and 14, responsible for the marked change in the  $250\text{-cm}^{-1}$  region of the calculated ROA forward-scattering spectrum of Fig. 13. For computational parameters, see Fig. 13; for definition of groups, see Fig. 9.

more than one stereogenic center, even in cases where more than one conformation of a chiral molecule comes into play.

No other spectroscopic method can provide chiral information comparable to that obtained from vibrational optical activity. While this is accepted wisdom for vibrational circular dichroism (VCD), our results show that the combined use of ROA measured

in forward- and back-scattering can do even better in this respect, particularly when the absolute configuration has to be determined for more than one stereogenic center. The observed sensitivity of ROA to the absolute configuration of a stereogenic center in a locally achiral environment disproves the currently held notion [37][38] that non-resonant ROA is inherently a short-range effect.

Apart from such stereochemical aspects, there are a number of findings of interest to molecular mechanics and to vibrational spectroscopy in general. The comparison of the vibrational modes of (4*S*)-**1** with those of the (4*S*)-isomers of **2** has, for the first time, revealed large-scale group vibrations on chiral molecular fragments. Such characteristic vibrational modes are better known for symmetric vibrational chromophores, and we also present evidence for characteristic vibrational motions persisting from benzene and *ortho*-xylene to **1** and **2**. Many more such correlations than presented here exist, and we have only discussed a small part of the wealth of information actually contained in the measured spectra and the computed data.

The availability of higher-quality calculations for the smaller (4*S*)-**1** has permitted us to validate the more-approximate calculations for the larger (4*S*)-**2**. A somewhat surprising result is that, by the judicious choice of computational methods, in particular DFT with hybrid functionals for the vibrational part, ROA spectra of a quality sufficient for stereochemical purposes can be obtained with extremely small basis sets for the electronic-tensor part. Useful qualitative agreement for small sets appears limited to wavenumber shifts below 1100 cm<sup>-1</sup>, and present experience indicates that it holds only for molecules with a predominantly hydrocarbon structure.

It is clear that more work remains to be done on the efficient computation of ROA data. The most sorely lacking piece are analytical gradients of the electronic tensors appearing in Eqn. 6. Once such analytical gradients become available, far better calculations than presented here will be possible for molecules of the size of *Galaxolide*®, or, conversely, similar-quality calculations for far larger molecules will become feasible. This will extend the scope of applicability for the determination of absolute configurations through comparison of measured and computed ROA data to an even wider range of practically important molecules than is possible at present.

We warmly thank Dr. Fridtjof Schröder (*Givaudan*) for reading and amending the manuscript, *Givaudan* (Switzerland) for providing samples of compounds **1** and **2**, Mr. Lukas Hesse (*Givaudan*) for preparing them, and the analytical division of *Givaudan* for analytical work. The measurement of the ROA spectrum of (4*S*)-*Galaxolide* (**2**) by Dr. Liqian Li is also gratefully acknowledged. This work was supported by grant 2000-066679 from the *Swiss National Science Foundation*.

## REFERENCES

- [1] L. D. Barron, 'Molecular Light Scattering and Optical Activity', Cambridge University Press, Cambridge, 1982.
- [2] L. A. Nafie, *Annu. Rev. Phys. Chem.* **1997**, 48, 357.
- [3] W. Hug, in 'Handbook of Vibrational Spectroscopy', Eds. J. M. Chalmers, P. R. Griffiths, John Wiley & Sons, Chichester, 2002, Vol. 1, p. 745.
- [4] P. K. Bose, L. D. Barron, P. L. Polavarapu, *Chem. Phys. Lett.* **1989**, 155, 423.
- [5] T. Helgaker, K. Ruud, K. L. Bak, P. Jørgensen, J. Olsen, *Faraday Discuss.* **1994**, 99, 165.
- [6] W. Hug, G. Zuber, A. de Meijere, A. F. Khlebnikov, H.-J. Hansen, *Helv. Chim. Acta* **2001**, 84, 1.
- [7] T. B. Freedman, X. Cao, R. K. Dukor, L. A. Nafie, *Chirality* **2003**, 15, 743.
- [8] G. Zuber, W. Hug, *J. Phys. Chem., A* **2004**, 108, 2108.

- [9] P. J. Stephens, F. J. Devlin, C. F. Chabalowski, M. J. Frisch, *J. Phys. Chem.* **1994**, 98, 11623.
- [10] H. Finkelmeier, R. Hopp, Pat. DE 8806200, Haarmann & Reimer, 1983.
- [11] G. Fräter, U. Müller, P. Kraft, *Helv. Chim. Acta* **1999**, 82, 1656.
- [12] W. Hug, H. Surbeck, *Chem. Phys. Lett.* **1979**, 60, 186.
- [13] L. Hecht, L. D. Barron, *Spectrochim. Acta, Part A* **1989**, 45, 671.
- [14] W. Hug, in 'Raman Spectroscopy, Linear and Nonlinear', Eds. J. Lascomb, P. Huang, Wiley-Heyden, Chichester, 1982, p. 3.
- [15] L. Hecht, L. D. Barron, W. Hug, *Chem. Phys. Lett.* **1989**, 158, 341; L. D. Barron, L. Hecht, W. Hug, M. J. MacIntosh, *J. Am. Chem. Soc.* **1989**, 111, 8731.
- [16] L. D. Barron, L. Hecht, A. R. Gargaro, W. Hug, *J. Raman Spectrosc.* **1990**, 21, 375.
- [17] L. D. Barron and J. R. Escibano, *Chem. Phys.* **1985**, 98, 437; K. M. Spencer, T. B. Freedman, L. A. Nafie, *Chem. Phys. Lett.* **1988**, 149, 367.
- [18] W. Hug, *Chem. Phys.* **2001**, 264, 53.
- [19] L. Hecht, L. A. Nafie, *Mol. Phys.* **1991**, 72, 441.
- [20] J. Oddershede, P. Jørgensen, D. L. Yeager, *Comput. Phys. Rep.* **1984**, 2, 33; P. Jørgensen, H. J. Aa. Jensen, J. Olsen, *J. Chem. Phys.* **1988**, 89, 3654.
- [21] T. Helgaker, H. J. Aa. Jensen, P. Jørgensen, J. Olsen, K. Ruud, H. Aagren, K. L. Bak, V. Bakken, O. Christiansen, P. Dahle, E. K. Dalskov, T. Enevoldsen, B. Fernandez, H. Heiberg, H. Hettema, D. Jonsson, S. Kirpekar, R. Kobayashi, H. Koch, K. V. Mikkelsen, P. Norman, M. J. Packer, T. A. Ruden, T. Saue, S. P. A. Sauer, K. O. Sylvester-Hvid, P. R. Taylor, O. Vahtras, DALTON, Version 1.1 (2000), an electronic structure program.
- [22] A. D. Becke, *J. Chem. Phys.* **1993**, 98, 5648; C. Lee, W. Yang, R. G. Parr, *Phys. Rev. B* **1988**, 37, 785.
- [23] GAUSSIAN98, *Gaussian Inc.*, Pittsburgh, PA.
- [24] G. Hangartner, FChk2 Hes (unpublished), University of Freiburg, Switzerland, 1997.
- [25] J. S. Binkley, J. A. Pople, W. J. Hehre, *J. Am. Chem. Soc.* **1980**, 102, 939.
- [26] F. London, *J. Phys. Radium* **1937**, 8, 397; R. Ditchfield, *Mol. Phys.* **1974**, 27, 789.
- [27] F. R. Dollish, W. G. Fateley, F. F. Bentley, 'Characteristic Raman Frequencies of Organic Compounds', John Wiley & Sons, New York, 1974.
- [28] N. B. Colthup, L. H. Daly, S. E. Wiberley, 'Introduction to Infrared and Raman Spectroscopy', 2nd edn., Academic Press, New York, 1975.
- [29] A. D. McLean, G. S. Chandler, *J. Chem. Phys.* **1980**, 72, 5639; R. Krishnan, J. S. Binkley, R. Seeger, J. A. Pople, *J. Chem. Phys.* **1980**, 72, 650.
- [30] P. C. Hariharan, J. A. Pople, *Theo. Chim. Acta* **1973**, 28, 213; R. Ditchfield, W. J. Hehre, J. A. Pople, *J. Chem. Phys.* **1971**, 54, 724.
- [31] W. Hug, G. Hangartner, *J. Raman Spectrosc.* **1999**, 30, 841.
- [32] W. Hug, *Appl. Spectrosc.* **2003**, 57, 1.
- [33] D. A. Long, 'The Raman Effect', John Wiley & Sons, Chichester, 2002.
- [34] W. Hug, A. Kamatari, K. Srinivasan, H.-J. Hansen, H.-R. Sliwka, *Chem. Phys. Lett.* **1980**, 76, 469.
- [35] W. Hug, S. Kint, G. F. Bailey, J. R. Scherer, *J. Am. Chem. Soc.* **1975**, 97, 5589.
- [36] H.-J. Hansen, H.-R. Sliwka, W. Hug, *Helv. Chim. Acta* **1979**, 62, 1120.
- [37] L. D. Barron, L. Hecht, A. F. Bell, G. Wilson, *Appl. Spectrosc.* **1996**, 50, 619; L. D. Barron, L. Hecht, E. W. Blanch, A. F. Bell, *Prog. Biophys. Mol. Biol.* **2000**, 73, 1.
- [38] L. A. Nafie, *Appl. Spectrosc.* **1996**, 50, 14.
- [39] K. Ruud, T. Helgaker, P. Bouř, *J. Phys. Chem., A* **2002**, 106, 7448.
- [40] T. Nakajima, S. Suga, T. Sugita, K. Ichikawa, *Tetrahedron* **1969**, 25, 1807.